QuadrantSearch: A Novel Method for Registering UAV and Backpack LiDAR Point Clouds in Forested Areas

Guorong Li, Bin Wu, *Member, IEEE*, Lei Yang, Zhan Pan, Linxin Dong, Siyu Wu, Guochun Shen, Jiarui Zhang, Tian Xiao, Lefeng Zhang, Jianping Wu, and Bailang Yu, *Senior Member, IEEE*

***Abstract*— Unmanned aerial vehicle (UAV) laser scanning (ULS) and backpack laser scanning (BLS) are two commonly employed technologies in precision forestry. However, data acquired by these two types of light detection and ranging (LiDAR) are distinct, with one capturing point clouds beneath the canopy and the other above. Consequently, there is minimal overlap in the point clouds collected by both methods, especially in dense forests, presenting significant challenges for data registration. Furthermore, many trees in forests (particularly broadleaf trees) have the tree tops and trunk centers not aligned vertically, which greatly increases the difficulty of the data registration methods based on tree position. To solve the above-mentioned problems, we here propose a novel and robust method to register ULS and BLS point clouds in forested areas. Our method consists of three key steps, that is, tree location extraction, quadrant search-based minimum spanning tree (MST) matching, and registration. The quadrant searching strategy dynamically searches for potential candidates in four quadrants centered on the initial tree locations. By constructing MSTs for the potential tree locations, triangle constraints require only four topologically similar tree locations to find one-to-one correspondences during the stepwise MST matching process. The proposed method was evaluated in five urban forest sample plots and one natural forest sample plot located in China, covering both coniferous and broadleaf forests. The results show that our method obtained good registration results on all six sample plots, with an averaged rotation error, translation error, pointwise error, and root-mean-square error (RMSE) of 0.012 rad, 0.354, 0.378, and 0.379 m, respectively. Comparative studies indicate that our method outperformed existing registration methods, demonstrating its effectiveness and robustness. Our method allows for the creation of a more complete picture of forest vertical structure and holds great potential for informing sustainable forest management practices and supporting critical ecological assessments.**

***Index Terms*— Backpack laser scanning (BLS), light detection and ranging (LiDAR), minimum spanning tree (MST), quadrant search, registration, unmanned aerial vehicle (UAV) laser scanning (ULS).**

I. Introduction

LIGHT detection and ranging (LiDAR) is a pivotal technique in forest surveys, offering significant advantages in the quantification and characterization of forest properties. LiDAR technology exhibits a broad spectrum of applications in the field of forestry, such as morphological parameters calculation (e.g., tree height, diameter at breast height, leaf area index, and crown diameter, etc.) [1], [2], [3], [4], 3-D tree modeling [5], [6], [7], urban greenness analysis [8], [9], forest inventory [10], [11], [12], and sustainable forest management [13], [14]. Currently, forestry mapping leverages LiDAR systems mounted on various platforms, including airborne, unmanned aerial vehicle (UAV)-borne, terrestrial, backpack, and handheld systems. The combination of these diverse platforms makes the acquirement of forest point clouds more comprehensive and precise, thereby offering superior data for forest management and inventory tasks.

The emerging UAV laser scanning (ULS), equipped with a global navigation satellite system (GNSS) and the inertial measurement unit (IMU), offers efficient capture of large-scale forest point clouds with georeferenced coordinates from an airborne perspective [15]. However, dense canopy cover often leads to signal transmission losses, limiting the laser sensors' ability to capture understory data [16]. Challenges associated with UAV flight above forest canopies result in incomplete or absent understory data. In contrast, the backpack/handheld laser scanning (BLS) system (hereinafter referred to as BLS) provides a unique capability to capture 3-D vegetation information from an understory perspective in a mobile manner and serves as a valuable complement to ULS point clouds [17], [18]. Currently, BLS systems typically utilize GNSS equipment and simultaneous localization and mapping (SLAM) techniques to acquire point clouds. In forested areas, trees often weaken or interrupt GNSS signals, posing challenges

Received 3 July 2024; revised 3 October 2024 and 26 November 2024; accepted 11 December 2024. Date of publication 16 December 2024; date of current version 27 December 2024. This work was supported in part by the National Key Research and Development Program of China under Grant 2023YFB3906101, in part by the Guangdong Basic and Applied Basic Research Foundation under Grant 2023A1515012487, and in part by the Baishanzu National Park Research Foundation under Grant 2021ZDLY03. *(Corresponding authors: Bailang Yu; Bin Wu.)*

Guorong Li, Lei Yang, Zhan Pan, Linxin Dong, Jiarui Zhang, Tian Xiao, Lefeng Zhang, Jianping Wu, and Bailang Yu are with the Key Laboratory of Geographic Information Science (Ministry of Education) and the School of Geographic Sciences, East China Normal University, Shanghai 200241, China (e-mail: 51253901074@stu.ecnu.edu.cn; 51203901080@stu.ecnu.edu.cn; 52283901042@stu.ecnu.edu.cn; 52283901045@stu.ecnu.edu.cn; 51213901096@stu.ecnu.edu.cn; 51213901058@stu.ecnu.edu.cn; 51263901072@stu.ecnu.edu.cn; jpwu@geo.ecnu.edu.cn; blyu@geo.ecnu.edu.cn).

Bin Wu is with the School of Geospatial Engineering and Science, Sun Yat-sen University, Zhuhai 519082, China (e-mail: wubin65@mail.sysu.edu.cn).

Siyu Wu and Guochun Shen are with Zhejiang Tiantong Forest Ecosystem National Observation and Research Station and the School of Ecological and Environments Sciences, East China Normal University, Shanghai 200241, China (e-mail: 52263903031@stu.ecnu.edu.cn; gcshen@des.ecnu.edu.cn).

Digital Object Identifier 10.1109/TGRS.2024.3518056

for obtaining accurate georeferenced point cloud data [19], [20]. In such cases, the SLAM technique allows BLS systems to capture point cloud data independently within a local coordinate system, providing valuable understory information. Nevertheless, SLAM-derived point clouds lack global georeferencing and cannot be directly integrated with the point clouds collected from ULS. Therefore, registering the ULS and BLS point cloud data is a prerequisite for obtaining complete and precise 3-D structural information on forests [3], [5], [21], [22].

Conventional methods for point cloud registration involve placing artificial markers with known georeferenced coordinates along the scanning route, which can be time-consuming and labor-intensive. Advances in automated and marker-free registration methods based on feature descriptors have demonstrated excellent performance in urban environments characterized by distinct geometric structures [23], [24], [25], [26], [27], [28]. However, such descriptors may prove less effective in forested environments where the lack of regular geometric structures in trees exacerbates the complexity. Moreover, owing to the different observation angles, there is limited physical overlap between the LiDAR data collected by ULS and BLS sensors, making it difficult to extract identical geometric features from both datasets. This challenge becomes more pronounced when the vertical view of BLS is limited. Therefore, many studies have proposed to utilize semantic overlapping information (such as tree location) for registration [5], [29], [30], [31], [32]. However, existing tree location-based methods are primarily tailored for coniferous trees (e.g., spruce and pine) or broadleaf trees with elliptic paraboloid shape and clear peaks (e.g., poplar and birch). These methods are challenging to generalize to broadleaf species, which have irregular canopies and their tops and trunk centers are not in the same vertical line [33].

In this work, we developed a novel method, *QuadrantSearch*, which is capable of performing point cloud registration in both coniferous and broadleaf forests. This method is an extension of our previous work [34], expanding our research scope from urban street scenes to forested environments. Specifically, this study offers two methodological contributions, including: 1) the development of a novel quadrant searching strategy to address the challenge of finding potential corresponding points from tree location maps in broadleaf forest scenarios and 2) the introduction of a robust triangle constraint algorithm to determine one-to-one correspondences between potential corresponding points. The rest of this article is structured as follows. Section II provides a review of related work. Section III introduces the methodology. Section IV describes the study area, data collection, experimental setup, and results. In Section V, we conducted a comparative experiment and discussed sensitivity analysis, computational efficiency, and limitations. Section VI draws the conclusions and the potential avenues for future research.

II. Related Work

Rigid 3-D point cloud registration methods can be broadly categorized into two categories: feature-based and deep learning-based. This section presents a brief overview of these two approaches, with a particular emphasis on their applications within forested ecosystems.

The general framework for feature-based methods involves three steps: feature extraction, feature description, and correspondence matching. The features extracted include both geometric and semantic attributes. Geometric features are typically the points, lines, and surfaces derived from point clouds using feature detectors such as local surface patches [35], intrinsic shape signatures [36], MeshDOG [37], 2.5-D scale-invariant feature transform (SIFT) [38], 3-D speeded up robust features (SURF) [39], 3-D Harris [40], and so on. However, these feature detectors are primarily designed for artificial and structured objects and may not be applicable in unstructured forest environments. To address this, Shao et al. [41] proposed a method for registering UAV and ground point clouds based on convex points of canopy contours. Ge et al. [42] proposed an approach to achieve registration by extracting feature descriptors of M dimensions across eight directions from the canopy profile skyline. In addition, some studies have employed mode points [5], [43] and visual occlusion points [44] to achieve effective matching, particularly in forest environments. However, these methods are sensitive to variations in point cloud density and require substantial physical overlap between two sets of point clouds. The quality of airborne and ground LiDAR data may not consistently meet these prerequisites.

Geometric feature-based methods fall short of leveraging the rich semantic information within point clouds. To address this shortcoming, numerous studies have incorporated forest-specific semantic information into the registration process, such as stem attributes [45], [46], canopy height [47], wood response [33], and tree location [29], [30], [31], [32], [34], [48], [49]. For instance, Wu et al. [34] proposed an effective method for registering vehicle-borne and backpack point clouds by leveraging the topological similarity of minimum spanning trees (MSTs) constructed from street tree trunks. This method identified potential correspondences based on tree topological relations, which were then pruned by identifying common subgraphs and expanded in a stepwise manner. Wang et al. [49] introduced a method for registering multiscan terrestrial laser scanning (TLS) data that employed the K-nearest neighbor algorithm to construct trunk triangles and conducted local matching based on triangle length similarity. However, the trunk-based methods are prone to failure due to the low overlap and insufficient trunk information in UAV point clouds [29]. In such cases, the crowns and trunks can be used as dependencies for extracting their common tree locations. Guan et al. [31] proposed using tree crown centers as designated tree locations in ULS data and matching them with BLS trunk centers employing a triangulated irregular network (TIN)-based framework. Polewski et al. [30] employed tree tops and trunk centers as tree locations. They created feature descriptors based on intertree distances to identify potential matched tree pairs and completed the ULS/BLS alignment by solving a maximum-weight matching problem within a bipartite graph. Hyyppä et al. [32] also used tree tops and trunk centers, constructing rotational- and translation-invariant descriptors based on the relative locations of neighboring trees.

The application of deep learning techniques to 3-D point cloud registration is a burgeoning research area. In comparison to methods relying on handcrafted features, deep learning-based methods exhibit greater potential in scenarios with extreme repetition, symmetrical elements, and high levels of noise [50], [51]. Pioneering approaches such as PointNet [52] and PointNet++ [53] directly extracted global and local features from raw, unordered point clouds, providing a learnable structured representation for such data. Building upon PointNet, PointNetLK [54] captured global features of 3-D point clouds and employed the iterative IC-Lucas-Kanade (LK) algorithm for feature matching. Deep closest point (DCP) [55] utilized a shared dynamic graph convolutional neural network (DGCNN) network to extract features from input point clouds, establishing connections between two sets of features using an attention module. These methods have shown promising results in small-scale indoor environments but face challenges when applied to large-scale outdoor scenarios due to feature extraction limitations [50]. JoKDNet [56] is the first deep learning-based method designed specifically for registering large-scale outdoor TLS data and demonstrated promising results on Wuhan University (WHU)-TLS and Eidgenössische Technische Hochschule (ETH)-TLS datasets. In addition, the innovative RoReg framework proposed by Wang et al. [57], which maximized the utilization of orientation descriptors and estimated local rotations, has also shown promise in the ETH dataset. Nonetheless, deep learning-based methods still face challenges, as they often demand a substantial volume of labeled training data, a resource currently limited for real outdoor scenes [48], [58]. Moreover, differences in data collection perspectives and point cloud density across different outdoor LiDAR platforms pose challenges for accurate inlier estimation in deep learning-based methods [50], [59].

Most existing geometric feature-based and deep learning-based methods often struggle to extract matching points from forest point clouds with limited physical overlap. Numerous studies have utilized semantic features, such as tree positions, to construct graph structures and subsequently extract corresponding descriptors for matching [31], [32], [34], [48], [49]. However, the vertical misalignment between tree tops and trunks, particularly in broadleaf forests, complicates the process of identifying potential corresponding points, while the complex forest environment leads to a large number of outliers in tree location data. To solve these challenges, we proposed a novel quadrant searching strategy to effectively identify potential correspondences and a robust triangle constraint algorithm to obtain one-to-one correspondences. Our proposed method circumvents the direct registration of tree positions. Instead, it employs a neighborhood search strategy to identify potential matching points based on tree locations, followed by the application of triangle constraints to obtain the final matching points. This approach effectively addresses the challenges posed by the vertical misalignment and the complex forest environment, ensuring accurate and reliable one-to-one correspondences.

III. Methodology

As shown in Fig. 1, the method we proposed takes as input a pair of point clouds from UAV and backpack and outputs a rigid transformation to register the ULS and BLS data. It consists of three main steps: tree location extraction, quadrant search-based MST matching, and registration, which are detailed as follows.

A. Tree Location Extraction

The registration primitives are determined based on the tree locations in our method. In contrast to the overlapping crowns, tree trunks are the most stable components in the forest, being distinct and easily detectable by ground LiDAR platforms. Therefore, we used the trunk centers as representative tree locations for BLS data. However, airborne LiDAR platforms often struggle to capture tree trunk information, thus tree locations were represented by tree crown tops. We employed two widely applicable individual tree detection algorithms to extract tree locations from point clouds. Specifically, for BLS data, the comparative shortest path algorithm proposed by Tao et al. [60] was used. The algorithm applies density-based spatial clustering of applications with noise (DBSCAN) for trunk clustering on point slices (10-cm vertical intervals) at a height of 1.3 m. The gravity center of each cluster is considered as the tree location. For ULS data, the layer stacking algorithm proposed by Ayrey et al. [61] was used to extract tree tops. This algorithm horizontally layers the forest canopy, filters out low vegetation by clustering each layer, and constructs an overlap map using the canopy height model (CHM). The local maxima of the overlap map are considered as the tree tops. The algorithm integrates the overlap map and CHM, ensuring effective detection results even in scenarios with low laser penetration [61]. The resulting individual tree coordinates (X, Y, and Z) are used as inputs for subsequent processing.

B. Quadrant Search-Based MST Matching

In this study, we assume that trees in a forest exhibit a unique spatial distribution pattern. The planar coordinates (i.e., X and Y) of the two sets of tree locations are utilized to construct MSTs using the Prim algorithm [62], [63], for matching [34]. However, as shown in Fig. 2, the tree top and trunk center are not aligned in the same vertical line in a broadleaf tree, registering UAV and backpack LiDAR point clouds using tree tops and trunk centers directly often leads to inaccurate transformation estimates. To address this problem, we have developed a novel quadrant-searching strategy that identifies potential correspondences by searching the possible neighborhoods surrounding the extracted tree locations.

1) Quadrant Searching: For ULS data, we generate a window of size T_g centered on the top of each tree, with T_g being a user-determined parameter specific to the tree type. This window is then divided into four quadrants, and the center point of each quadrant is considered as a potential candidate (potential tree location) instead of the original tree top for matching with the trunk centers obtained from BLS data. For example, a selected candidate for a tree top V_0^A can be represented as follows:

$$V_{0_\xi}^A \in \left\langle V_{0_{\mathrm{ur}}}^A, V_{0_{\mathrm{ul}}}^A, V_{0_{\mathrm{ll}}}^A, V_{0_{\mathrm{lr}}}^A \right\rangle \tag{1}$$

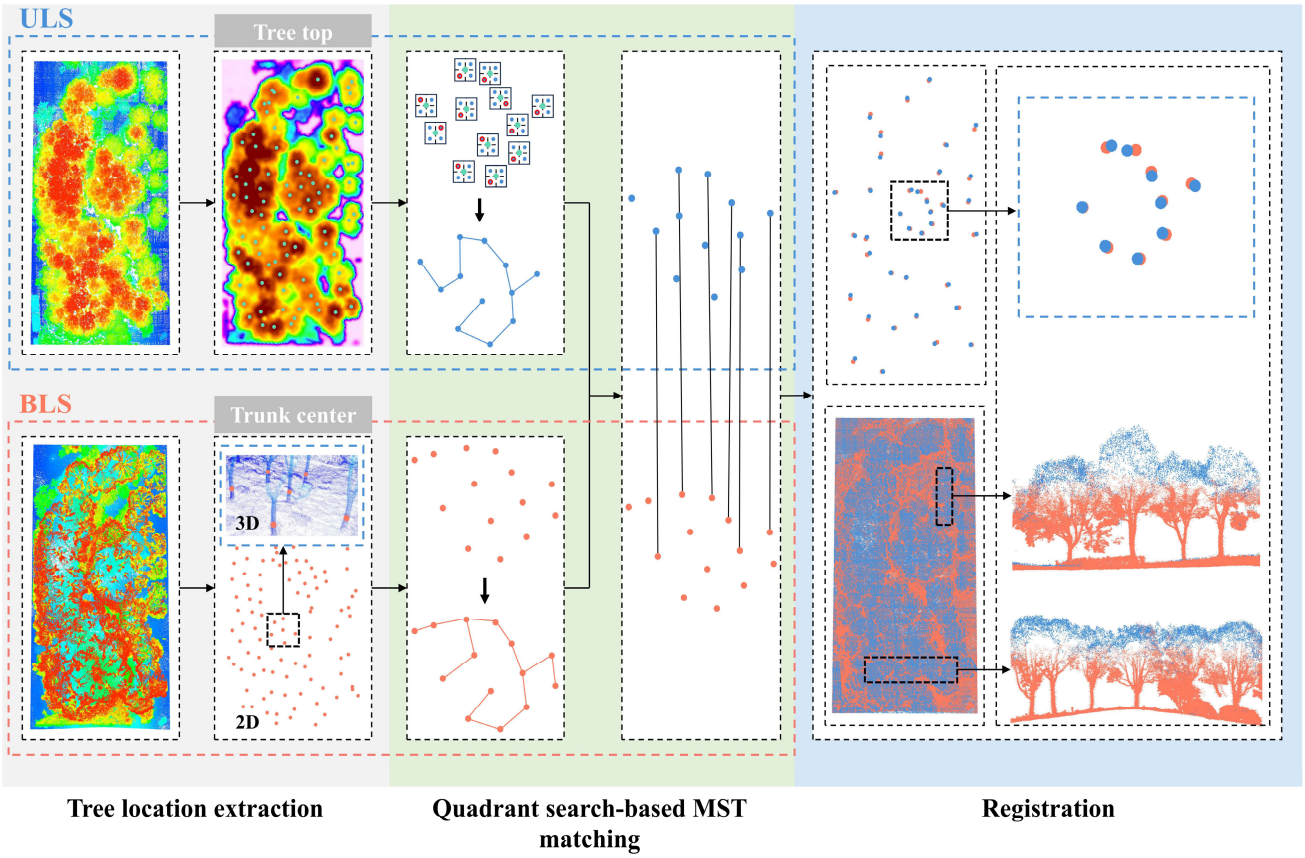

Fig. 1. Workflow of the proposed method for registering ULS and BLS data.

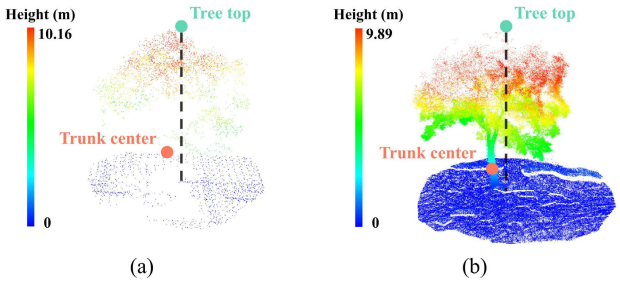

(a) (b)

Fig. 2. Discrepancy between the tree planar locations from (a) ULS and (b) BLS when the tree top and trunk center are not aligned in the same vertical line.

where $V^A_{0_{\text{ur}}}$, $V^A_{0_{\text{ul}}}$, $V^A_{0_{\text{ll}}}$, and $V^A_{0_{\text{lr}}}$ are the potential candidates located in the center of the upper-right, upper-left, lower-left, and lower-right quadrants, respectively. $V^A_{0_\xi}$ represents the selected candidate and can be any one of $V^A_{0_{\text{ur}}}$, $V^A_{0_{\text{ul}}}$, $V^A_{0_{\text{ll}}}$, and $V^A_{0_{\text{lr}}}$.

We illustrate the quadrant searching process of a single tree as an example in Fig. 3(a). This process begins with the input of the tree top V^A_0 from ULS data, followed by the generation of four potential candidates ($V^A_{0_{\text{ur}}}$, $V^A_{0_{\text{ul}}}$, $V^A_{0_{\text{ll}}}$, and $V^A_{0_{\text{lr}}}$). The objective is to iteratively select the candidate that yields the most optimal match with the trunk center of the corresponding tree in the BLS data. The best candidate from each iteration is subsequently fed into the next iteration as a basis for generating further candidates, such as $V^A_{0_{\text{ll}}}$, $V^A_{0_{\text{ll,ul}}}$, and $V^A_{0_{\text{ll,ul,ll}}}$. As illustrated in Fig. 3(b), the selected candidates in each iteration will be used to construct the MSTs, such as MST^{A_1}, MST^{A_2}, MST^{A_3}, and so on. Theoretically, 4^l combinations of potential candidates could be selected, where l represents the number of trees. These MSTs are then matched with the MST^B using the graph similarity. To find the optimal match, we here define a fitness score to evaluate the matching results

$$\mathcal{F} = n_m \times \left(\delta_{\text{avg}} - d_{\text{avg}}\right) \tag{2}$$

where n_m is the number of matched node pairs, d_{avg} represents the average distance between these n_m pairs (after transformation into a common coordinate system), and δ_{avg} is a constant with a value of T_d in the first iteration. In the subsequent iteration, it is defined as the average distance between pairs of best-matching nodes from the previous iteration.

Based on this equation, we aim to solve a combinatorial problem involving the selection of optimal potential candidates from the ULS point clouds. To this end, we employed the genetic algorithm metaheuristic, which is a general scheme for maximizing (2) and efficiently identifying the global optimal match between two datasets. As illustrated in Fig. 3(c), this process is initiated by randomly generating a selected candidate combination set (including k MSTs), followed by sequential MST matching. The evolution of the combination set proceeds through biologically inspired operators: selection, crossover, and mutation, which are guided by the fitness scores. This evolution procedure continues until the specified

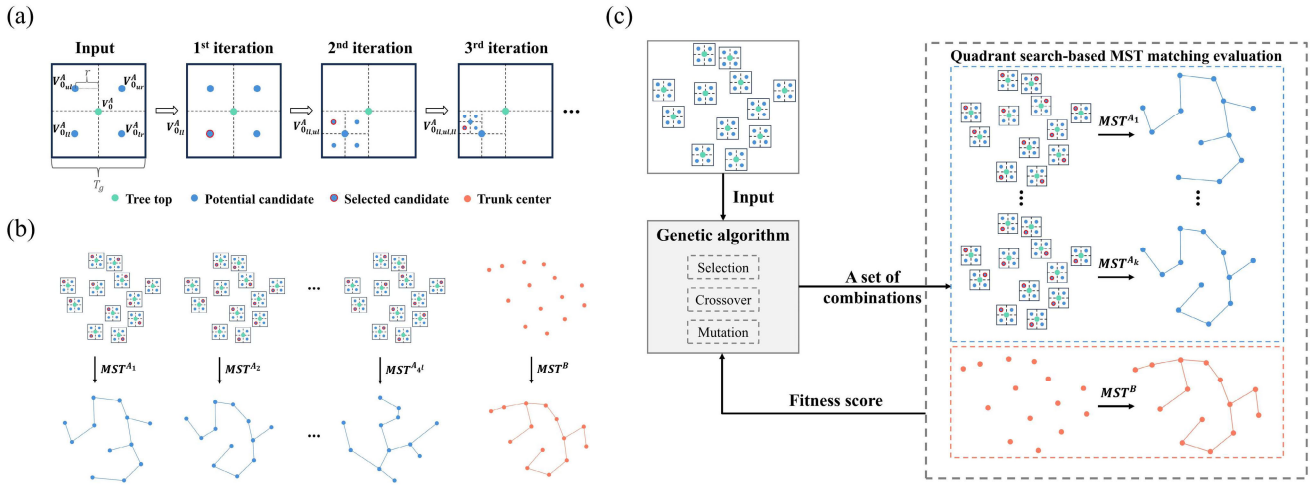

Fig. 3. (a) Illustration of the quadrant searching process of a single tree, (b) MST construction process in each iteration, and (c) quadrant search-based MST matching process driven by the genetic algorithm. r is used to compute the coordinates of the candidates with a value equal to 1/4 of T_g.

maximum number of generations is reached. Upon completion, the best combination with the highest fitness score is selected as the output. The matched node pairs derived from this process are then used as input for the next iteration. This iterative procedure is repeated until reaching T_N iterations, at which point the final matched node pairs are obtained.

2) Node Similarity Matching: The matching between two MSTs in the quadrant searching process is based on the distance and angle similarity between their nodes. We define the topological property P_i of a node V_i in an MST as

$$P_i = \begin{cases} \{D_{i,1}\}, & m = 1 \\ \{D_{i,1}, D_{i,2}, \ldots, D_{i,m}; \theta_{i,1}, \theta_{i,2}, \ldots, \theta_{i,n}\} \\ \qquad m \geq 2, \quad n = C_m^2 \end{cases} \tag{3}$$

where m is the number of neighboring edges of the node V_i, θ represents the included angle of every two edges that are connected with the node V_i, and D_i represents the Euclidean distance between the connected nodes. Two nodes can be considered as a pair of similar nodes if their properties satisfy the following constraints:

$$\begin{cases} m = p \\ \left|D_{0,k}^A - D_{0,k}^B\right| \leq T_\lambda, \quad (k = 1, 2, \ldots, m) \\ \left|\theta_{0,s}^A - \theta_{0,s}^B\right| \leq T_\mu, \quad \left(s = 1, 2, \ldots, n, n = C_m^2\right) \end{cases} \tag{4}$$

where m and p represent the number of neighboring edges of the two nodes, respectively. Node similarity comparison is feasible only when $m = p$. Two nodes are considered similar when the difference between the edge lengths of two nodes is less than T_λ and the difference between the angles is less than T_μ [64]. T_λ and T_μ are user-defined thresholds and will be specified in Section IV.

3) Correspondence Pruning: Based on node similarity, we can obtain initial correspondences that can be either one-to-one or one-to-many. Refinement of the initial correspondences is essential to reliable point cloud registration. Several strategies have been employed to achieve this goal, such as common subgraphs [34], [48], the largest consensus set [49], and random sample consistency (RANSAC)-based approaches [31], [33]. However, in structurally diverse forests, it is usually difficult to extract small trees from airborne LiDAR data [65], and over-segmentation and under-segmentation occur frequently during the individual tree segmentation process. In such cases, the tree location maps contain numerous outliers, and only a small number of discretely distributed initial correspondences can be obtained. Tasks such as identifying common subgraphs or determining the largest consensus set require initial correspondences to be connected within the graph structure with a guaranteed number. Additionally, excessive outliers can impede the convergence of RANSAC-based approaches. Therefore, we developed a robust pruning algorithm tailored to this scenario. The algorithm is technically simple and leverages the topological relationship between a triangle and an additional node to constrain the matching process. It requires only four pairs of discretely distributed initial correspondences to efficiently complete the pruning operation.

Specifically, in the source corresponding point set, we select three nodes to construct a triangle and seek the corresponding triangle in the target corresponding point set based on the side lengths of the triangle. Here, we define the similarity of a pair of triangles by the following equation:

$$S\left(t^A, t^B\right) = \max \left|l_i^A - l_i^B\right| \leq T_\lambda, \quad i = 1, 2, 3 \tag{5}$$

where $S(t^A, t^B)$ represents the topological similarity of two triangles t^A and t^B. l_i^A and l_i^B are the lengths of the corresponding edges in the two triangles. T_λ is the same threshold used for node similarity comparison and represents the maximum allowed difference in edge length for two triangles to be matched.

However, the matching of two triangles does not guarantee that the nodes comprising these triangles correspond in a one-to-one manner. For example, as illustrated in Fig. 4(a), based on length similarity, triangle t_1^A has two corresponding triangles: t_1^B and $t_{1'}^B$. To achieve a one-to-one match, additional

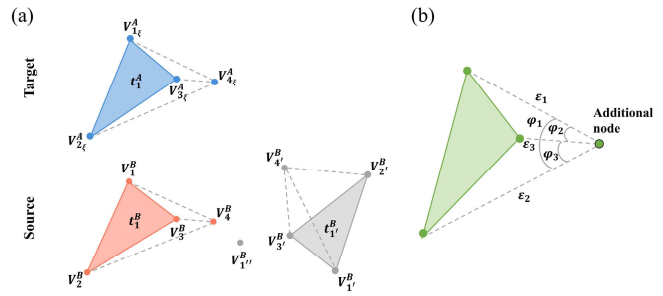

Fig. 4. (a) Example illustrating the robust triangle constraint process and (b) schematic illustration of the feature descriptor with six dimensions.

nodes are introduced after completing triangle matching to connect with these triangles, thereby constructing the feature descriptors illustrated in Fig. 4(b). The feature descriptor is defined as

$$f_{\text{tri\_addi}} = (\varepsilon_1, \varepsilon_2, \varepsilon_3, \varphi_1, \varphi_2, \varphi_3) \tag{6}$$

where ε_1, ε_2, and ε_3 represent the lengths of the three edges formed by connecting the additional node with the triangle's vertices, while φ_1, φ_2, and φ_3 denote the angles formed by ε_1, ε_2, and ε_3 with the additional node. Two similar feature descriptors should satisfy the following conditions:

$$\begin{cases} \left|\varepsilon_i^A - \varepsilon_i^B\right| \le T_\lambda, & i = 1, 2, 3 \\ \left|\varphi_j^A - \varphi_j^B\right| \le T_\mu, & j = 1, 2, 3 \end{cases} \tag{7}$$

where T_λ and T_μ are the same thresholds used for the node similarity calculation. In Fig. 4(a), the descriptor constructed from t_1^A and $V_{4_\xi}^A$ exhibits similarity to the descriptor constructed from t_1^B and V_4^B, while exhibiting distinctiveness when compared to descriptors constructed from $t_{1'}^B$ and V_4^B or $V_{4'}^B$. As a result, the four pairs of one-to-one correspondences $(V_{1_\xi}^A, V_1^B)$, $(V_{2_\xi}^A, V_2^B)$, $(V_{3_\xi}^A, V_3^B)$, and $(V_{4_\xi}^A, V_4^B)$ are matched.

The pseudocode for the robust triangle constraint algorithm is provided in Algorithm 1. The time complexity for calculating all combinations step is $O(k^3)$, the time complexity of edge matching is $O(k)$, and the time complexity of the descriptor matching process is also $O(k)$, where k relates to the number of corresponding points in each unpruned correspondence.

4) Correspondence Expansion: Following the strategy proposed by Wu et al. [34], the four pairs of correspondences obtained in the previous step are progressively expanded through a stepwise matching process to enhance matching accuracy. This involves applying the initial transform matrix calculated from the established one-to-one correspondences to transform the unmatched nodes. Subsequently, the search for topologically similar nodes is conducted within a specified neighborhood threshold T_ε surrounding the transformed nodes. The final matched node pairs are obtained by iterating over all unmatched nodes.

Algorithm 1 Robust Triangle Constraint Algorithm

Input: Initial correspondences $\{\boldsymbol{V}_{sim}^{A}, \boldsymbol{V}_{sim}^{B}\}$; Length and angle threshold $\boldsymbol{TH}$ between two descriptors
Output: One-to-one correspondences $\{\boldsymbol{V}_{corr}^{A}, \boldsymbol{V}_{corr}^{B}\}$
Initialization: $\boldsymbol{V}_{corr}^{A} \leftarrow \emptyset$; $\boldsymbol{V}_{corr}^{B} \leftarrow \emptyset$; $\boldsymbol{foundmatch} \leftarrow False$

```
for i = 1 to size(V^A_sim) − 3 do
    U ← calculate all combinations(V^B_sim,i:i+2)
    for each u ∈ U do
        M^A, M^B ← edge matching(V^A_sim,i:i+2, u)
    end for
    if size(M^A) > 0 do
        desc^A ← calculate descriptor(M^A, V^A_sim,i+3)
        for each m^B ∈ M^B do
            desc^B ← calculate descriptor(m^B, V^B_sim,i+3)
            if |desc^A − desc^B| ≤ TH do
                V^A_corr ← m^A
                V^B_corr ← m^B
                foundmatch ← True
                break
            end if
        if foundmatch do
            break
        end for
    end if
    if foundmatch do
        break
end for
```

C. Registration

Through the matching process described above, we can obtain a set of planar coordinates (i.e., X and Y) from the matched node pairs. To achieve 3-D registration, the Z-coordinates need to be calculated. First, we applied the cloth simulation filter algorithm [66] to filter the ground points within both sets of the original point clouds. Then, we calculated the average elevations of all ground points within a 1-m buffer around the projection of the matched node pairs onto the ground. Finally, these average elevations were assigned as the Z-coordinates for the matched node pairs, calculated using the following equation:

$$\mathcal{Z} = \frac{1}{p_n} \sum_{i}^{p_n} p_{i,z} \tag{8}$$

where $p_{i,z}$ represents the Z-coordinate of a ground point located within the 1-m buffer and p_n indicates the number of ground points in the buffer.

The 3-D coordinates of the matched node pairs allow for the estimation of the transformation between ULS point cloud data X^A and BLS point cloud data X^B. The transform matrix $\boldsymbol{T}$ with 6° of freedom can be parameterized by a rotation matrix $\boldsymbol{R} \in \mathbb{R}^{3\times3}$ and a translation vector $\boldsymbol{t} \in \mathbb{R}^3$ as follows:

$$\boldsymbol{T} = \begin{bmatrix} \boldsymbol{R} & \boldsymbol{t} \\ \boldsymbol{0}^{\mathrm{T}} & \boldsymbol{1} \end{bmatrix} = \begin{bmatrix} R_{11} & R_{12} & R_{13} & t_x \\ R_{21} & R_{22} & R_{23} & t_y \\ R_{31} & R_{32} & R_{33} & t_z \\ 0 & 0 & 0 & 1 \end{bmatrix}. \tag{9}$$

The rotation matrix and translation vectors can be realized by singular value decomposition [67]. Therefore, the relationship between the two sets of point cloud registration can be

described as

$$X^A = \boldsymbol{R}(x, y, z)X^B + \boldsymbol{t}(1:3). \tag{10}$$

Additionally, fine registration algorithms such as the iterative closest point (ICP) algorithm [68] were also considered in our study. However, the optimization effect of this algorithm is influenced by the degree of physical overlap between two datasets, a subject that is explored in greater detail in Section IV-E.

D. Accuracy Assessment

To evaluate the accuracy of tree location extraction, we compare the number of trees extracted by the individual tree detection algorithm with the reference number of trees that were manually marked using LiDAR360 software (https://www.lidar360.com). Then, three accuracy statistics, namely recall (r), precision (p), and F-score (F) were calculated.

To evaluate our registration results, we manually selected 10–20 pairs of corresponding points from the target and source point clouds to obtain the reference transformation. We conducted separate evaluations for coarse registration and fine registration, recording matrix-based errors, pointwise errors, and root-mean-square errors (RMSEs). In addition, we also calculated the success rate of matched tree pairs.

Matrix-based errors, including rotation error E_R and translation error E_t, can be calculated using the transform matrix T estimated by our algorithm and the reference transform matrix T^G

$$\begin{cases} \Delta T = T\left(T^G\right)^{-1} = \begin{bmatrix} \Delta R & \Delta t \\ 0^{\mathrm{T}} & 1 \end{bmatrix} \\ E_R = \arccos\left(\dfrac{\mathrm{tr}(\Delta R) - 1}{2}\right) \\ E_t = \|\Delta t\| \end{cases} \tag{11}$$

where ΔR and Δt are the rotational and translational components of the residual transformation ΔT, and tr(•) is the trace of a matrix.

Pointwise error E_p provides a more intuitive measure for comparing differences between the estimated and reference transformation matrices. By selecting 100 randomly points p_r from the source point cloud, the pointwise error is defined as

$$E_p = \frac{1}{100}\sum_{i=1}^{100}\left\|T^G p_{r,i} - T p_{r,i}\right\|. \tag{12}$$

RMSE is used to further evaluate the registration results and is defined as

$$\mathrm{RMSE} = \sqrt{\frac{\sum_{(p^s, p^t)\in C^G}\|T p^s - p^t\|^2}{\left|C^G\right|}} \tag{13}$$

where C^G represents several pairs of corresponding points manually selected from the target and source point clouds, p^s and p^t denote a pair of corresponding points from C^G.

The success rate of matched tree pairs is determined by the ratio of tree pairs identified by our algorithm to the manually identified reference matches. Moreover, the greater the number of successfully matched tree pairs, the higher the accuracy of the match.

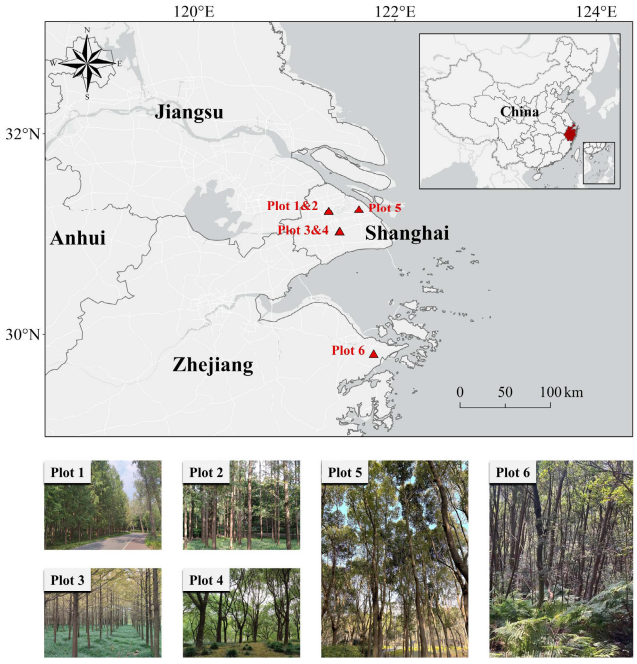

Fig. 5. Locations and photographs of the six sample plots.

IV. Experimental Analyses

A. Study Area

Six sample plots were used to validate the applicability of the proposed method, with five situated in Shanghai (Plots 1–5) and one (Plot 6) located in Zhejiang Province, as depicted in Fig. 5. Plots 1 and 2 are located in Changning Greenway Park within the Changning District, Shanghai, predominantly populated by *Metasequoia glyptostroboides*, *Populus L*, and *Acer grandidentatum* as the main tree species. Plots 3 and 4 are situated on the campus of East China Normal University (ECNU) in the Minhang District, Shanghai, featuring *M. glyptostroboides* and *Cinnamomum camphora* as the primary tree species, respectively. Plot 5 is located in the Jinhai Wetland Park in the Pudong District of Shanghai, where *C. camphora* is the dominant tree species. Plot 6 is positioned in Zhejiang Tiantong National Forest Park, where the principal tree species are broadleaf trees such as *Castanopsis fargesii*, *Schima superba*, and *Choerospondias axiliaris*. These sample plots include both urban and natural forest settings, characterized by varying tree densities and topography. Specifically, Plots 1–3 are covered with wild grass and feature a flat terrain, with both Plots 1 and 2 intersected by a road. Plots 4 and 5 are distinguished by low shrubs and undulating surfaces. Plot 6 is characterized by dense shrubs reaching breast height and humped surfaces, introducing increased registration challenges relative to the other plots. The details and data information for the sample plots are provided in Tables I and II, respectively.

B. LiDAR Data

The ULS data were collected by a RIEGL miniVUX-1 UAV laser scanner mounted on a FEIMA D200 quadcopter UAV platform, which carried both GNSS and a high-precision IMU. The RIEGL miniVUX-1 scanner operates in the near-infrared

TABLE I
DETAILS OF THE SIX SAMPLE PLOTS

Forest sites	Plots	Dominant tree species	Tree height (m)	diameter at breast height (cm)	Stem density (trees/ha)	Area (m^2)
Changning Greenway Park	1	*Metasequoia glyptostroboides*, *PopulusL*	19	19	789	30×30
	2	*Metasequoia glyptostroboides*, *Acer grandidentatum*	13	21	811	30×30
ECNU Campus	3	*Metasequoia glyptostroboides*	11	15	2325	20×20
	4	*Cinnamomum camphora*	12	51	155	110×55
Jinhai Wetland Park	5	*Cinnamomum camphora*	12	21	466	70×50
Tiantong National Forest Park	6	*Castanopsis fargesii*, *Schima superba*, *Choerospondias axiliaris*	14	33	~2000	50×50

TABLE II
DATA INFORMATION OF THE SIX SAMPLE PLOTS

Plots	Dominant tree types	Nuisances	Overlap rates (%)
1	Coniferous trees	Additional man-made clutter	28.14
2	Coniferous trees	Additional man-made clutter	22.76
3	Coniferous trees	Limited overlap, low shrubs	8.33
4	Broadleaf trees	Limited overlap, low shrubs, undulating surfaces	8.25
5	Broadleaf trees	Limited overlap, low shrubs, undulating surfaces	13.28
6	Broadleaf trees	Dense and high shrubs, humped surfaces	26.17

TABLE III
DATA ACQUISITION PARAMETERS AND SPECIFICATIONS FOR ULS AND BLS

Parameters	ULS	BLS	
	miniVUX-1	Libackpack 50	Zeb Horizon
Altitude	70~100 m	~2 m	~1.5 m
Speed	5 m/s	1 m/s	1 m/s
Maximum range	330 m	100 m	100 m
Accuracy	15 mm	30 mm	6 mm
Wavelength	near-infrared	903 nm	903 nm
Horizontal field of view	360°	360°	360°
Vertical field of view	/	30°	270°
Scan frequency	100,000 pts/s	300,000 pts/s	300,000 pts/s

wavelength range and has a maximum measurement range of 330 m. The UAV platform flew along zigzag courses at an altitude of approximately 100 m in Plots 1–5 and 70 m in Plot 6 above the ground, ensuring an overlap of more than 80% between flight lines across all plots. The average point density of the collected UAV LiDAR data is about 65 points/m^2 in Plots 1–5 and 399 points/m^2 in Plot 6. The point cloud data were georeferenced to the world geodetic system (WGS) 84 datum and projected to a planar coordinate system of universal transverse mercator (UTM) (Zone 51N). Table III provides further details about the specifications of the ULS system.

The GreenValley LiBackpack 50 system and the GeoSLAM Zeb Horizon system were utilized for understory data collection. The LiBackpack 50 system is equipped with a Velodyne VLP-16 laser scanner, a panoramic camera, a motherboard backpack, and a handheld touchpad. The Velodyne VLP-16 scanner provided a horizontal field of view of 360° and a vertical field of view of 30° (from −15° to 15°). It was used to collect BLS data for Plots 3–5. The Zeb-Horizon scanner is a BLS device mounted on a rotating arm, with a datalogger carrier as a backpack or shoulder strap. It provides a horizontal field of view of 360° and a vertical field of view of 270°, enabling it to capture richer information about the vegetation canopy. It was used to collect BLS data for Plots 1, 2, and 6. The average point density of the collected BLS data is approximately 5375 points/m^2 in Plots 3–5, and 38 005 points/m^2 in Plots 1, 2, and 6. Additional details about the BLS system can be found in Table III.

C. Experimental Setup

Before executing our registration algorithm, we preprocessed the point cloud data using the LiDAR360 software. The initial steps involved denoising the raw point clouds and filtering the ground points. Subsequently, a height normalization operation was applied to the point cloud data, using ground points as the references. The normalized data were then used as input for individual tree detection. It should be noted that

TABLE IV
SUMMARY OF PARAMETERS USED IN THE PROPOSED METHOD

Parameters	Descriptions	Plots	Values
T_λ	The distance threshold for defining the node similarity	Plots 1-3 Plots 4-6	0.8 m 2 m
T_μ	The angle threshold for defining the node similarity	Plots 1-3 Plots 4-6	8° 12°
T_ε	The threshold for search radius	Plots 1-6	3 m
T_g	The initial quadrant searching window size	Plot 1 Plots 2, 3 Plots 4-6	1.25 m 1 m 2 m
T_d	The initial average distance threshold for matched node pairs	Plots 1-3 Plots 4-6	1 m 1.5 m
T_N	The max number of iterations	Plots 1-6	3

TABLE V
ACCURACY ASSESSMENT OF THE TREE LOCATION EXTRACTION RESULTS ON THE SIX SAMPLE PLOTS

Plots	Data	Ref.	Et.	TP	FP	FN	r	p	F
1	BLS	71	70	68	2	3	0.958	0.971	0.965
	ULS	70	60	52	8	18	0.743	0.867	0.800
2	BLS	73	68	57	11	16	0.781	0.838	0.809
	ULS	73	45	44	1	29	0.603	0.978	0.746
3	BLS	91	90	85	5	6	0.934	0.944	0.939
	ULS	93	79	72	7	21	0.774	0.911	0.837
4	BLS	94	131	85	46	9	0.904	0.649	0.756
	ULS	94	85	75	10	19	0.798	0.882	0.838
5	BLS	163	174	161	13	2	0.988	0.925	0.955
	ULS	163	147	125	22	38	0.767	0.850	0.806
6	BLS	64	76	46	30	18	0.719	0.605	0.657
	ULS	64	66	29	37	35	0.453	0.439	0.446
Avg.	BLS	93	102	84	18	9	0.881	0.822	0.847
	ULS	93	80	66	14	27	0.690	0.821	0.746

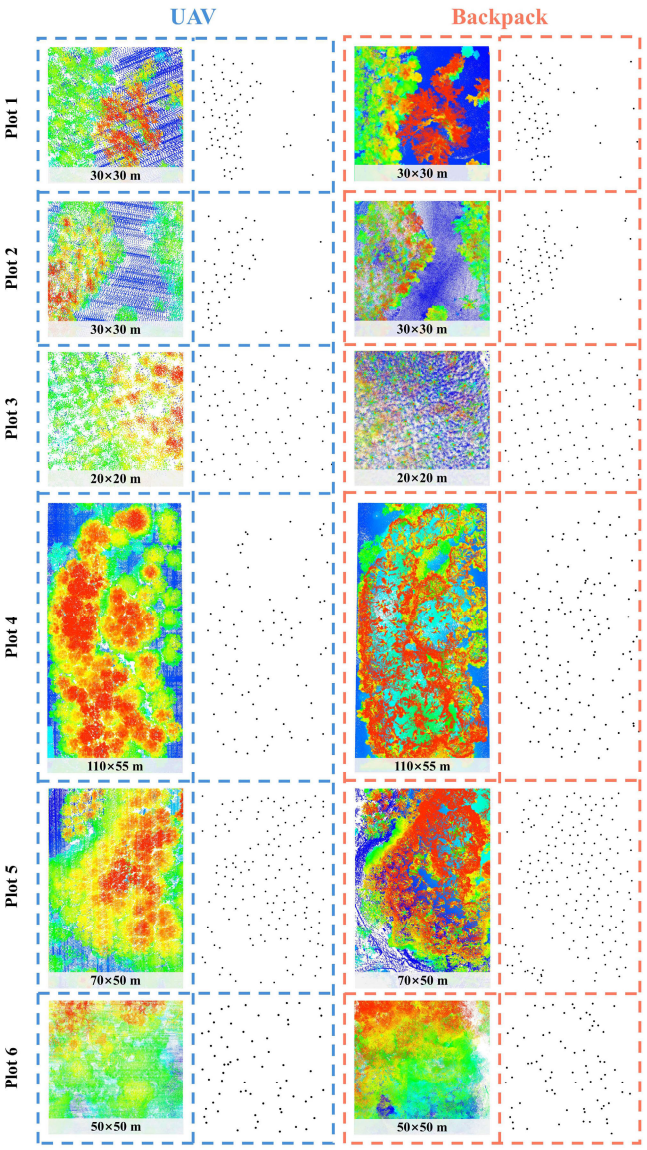

Fig. 6. Collected (left) UAV and (right) backpack LiDAR data on the six sample plots, along with their corresponding individual tree detection results indicated by black dots.

to mitigate the impact of varying data collection viewpoints on tree location maps, we selected to include only trees with heights greater than 15 m for registration in Plot 6, given its complex and multilayered vertical canopy structure. Finally, the extracted tree locations are used as input to the proposed algorithm to achieve absolute coordinate transformation from BLS data to ULS data. All experiments are executed on a desktop computer with an Intel Core i7-12700 CPU, 2.10 GHz, and 32 GB RAM, running a Windows 11, 64-bit operating system. All the parameter settings are given in Table IV.

D. Tree Location Extraction Results

The accuracy assessment of the extracted tree locations for the six sample plots was summarized in Table V. Et. and Ref., respectively, representing the extracted trees and reference trees. Overall, the accuracy of tree location extraction was satisfactory, with average F-scores of 0.847 and 0.746 for BLS and ULS data, respectively. Specifically, lower F-scores for BLS data compared to ULS data were observed in Plot 4, which may be attributed to the irregular stem diameters. For Plots 1–5, both BLS and ULS data yielded F-scores exceeding 0.7. However, for Plot 6, both datasets exhibited lower F-scores, likely influenced by the undulating ground surfaces, dense shrubs, and the complex vertical structure of the forest. The point clouds and the extracted tree locations are shown in Fig. 6.

E. Registration Results

Table VI summarizes the accuracy of the registration results for the six sample plots. It indicates that 25, 19, 15, 37, 54, and 12 correspondences were successfully matched, with success rates of about 50%. The potential reasons for the relatively low matching rates may stem from erroneous tree segmentation of airborne LiDAR data and the existence of small trees, resulting in a limited number of tree locations available for

TABLE VI
ACCURACY OF THE REGISTRATION RESULTS ON THE SIX SAMPLE PLOTS

Plots	Potential matches	Final matches	Success rate (%)	Coarse registration errors				Fine registration errors			
				E_R (*rad*)	E_t (m)	E_p (m)	*RMSE* (m)	E_R (*rad*)	E_t (m)	E_p (m)	*RMSE* (m)
1	51	25	49	0.008	0.178	0.194	0.156	0.003	0.091	0.094	0.096
2	40	19	48	0.011	0.408	0.410	0.412	0.024	0.050	0.335	0.331
3	30	15	50	0.009	0.329	0.406	0.395	0.019	0.431	0.438	0.429
4	74	37	50	0.003	0.296	0.310	0.380	0.004	0.345	0.345	0.398
5	108	54	50	0.007	0.577	0.274	0.224	0.012	0.766	0.275	0.288
6	28	12	43	0.035	0.336	0.676	0.708	0.014	0.264	0.308	0.361
Avg.	55	27	48	0.012	0.354	0.378	0.379	0.013	0.325	0.299	0.317

matching. The coarse registration results demonstrate that the proposed method achieved satisfactory accuracy in urban forests (Plots 1–5), while the accuracy in natural forests (Plot 6) is comparatively lower but acceptable. The overall average rotation error, translation error, pointwise error, and RMSE of 0.012 rad, 0.354, 0.378, and 0.379 m. Additionally, we performed fine registration using the ICP algorithm [68] on the coarse registration results and calculated the evaluation metrics.

Fig. 7 illustrates the coarse and fine registration results of our proposed method on the six sample plots. Close-up views of each plot demonstrate the accurate registration of ULS and BLS point clouds from distinct forest environments. For Plots 1 and 2, located in a park as depicted in Fig. 7(a) and (b), the coarsely aligned BLS point cloud (red) already exhibits a good match with the ULS point cloud (blue). However, the finely aligned BLS point cloud (green) further optimized the registration between the two sets of point clouds. Plots 3–5, as shown in Fig. 7(c)–(e), demonstrate successful matching despite limited physical overlap between the two sets of point clouds. In this case, fine registration is redundant, and the difference between the coarse and fine registrations is imperceptible in the figures. Plot 6, located in a mountainous area with a complex forest environment, exhibits larger registration errors compared to the plots in the urban forests. Nevertheless, the algorithm is capable of achieving good registration even in the absence of fine registration.

Overall, by combining several evaluation metrics (Table VI) and the visual effect of registration (Fig. 7), we found that the fine registration did not improve the registration accuracy for Plots 3–5, and even caused a slight decrease in accuracy. It can be attributed to the fact that our method successfully identified an adequate number of representative correspondences, ensuring that its accuracy was not necessarily inferior to fine registration. Besides, the efficacy of fine registration actually depends on the quality of the collected data. In Plots 3–5, the ground data were collected using a backpack device with an accuracy of 30 mm, which is lower than the 15 mm accuracy achieved with the airborne device. Furthermore, the backpack's restricted vertical field of view (−15° to 15°) limited the physical overlap between the datasets, increasing the likelihood of encountering mismatching errors in the ICP results and introducing an additional source of bias. In contrast, for Plots 1, 2, and 6, the ground data were collected using a handheld device with a 270° vertical field of view and 6 mm accuracy. The ICP algorithm improved the coarse registration results due to the sufficient physical overlap between the

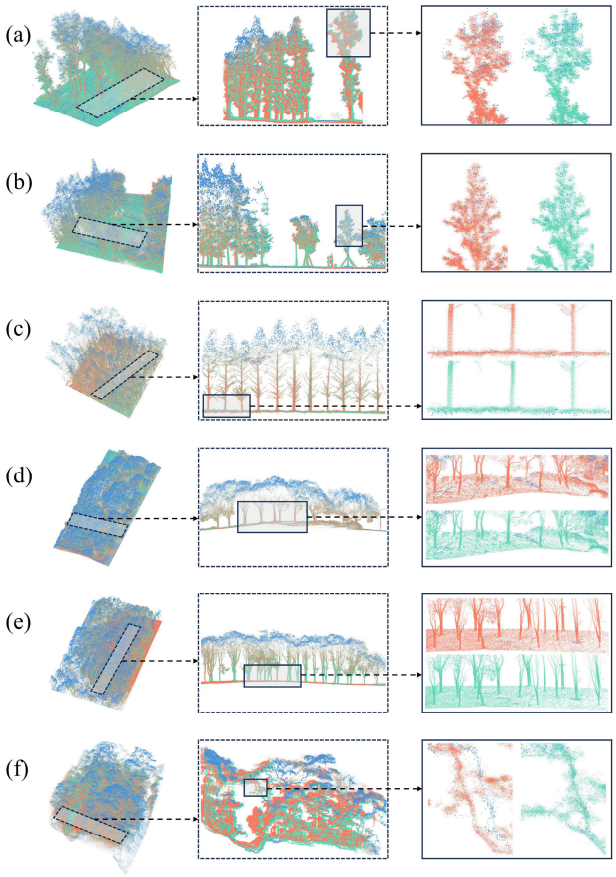

Fig. 7. Registration results for (a)–(f) Plot 1, Plot 2, Plot 3, Plot 4, Plot 5, and Plot 6, respectively. The blue point clouds represent the ULS data, while the red and green point clouds denote the coarsely and finely registered BLS data, respectively.

TABLE VII
ACCURACY COMPARISON WITH SIX COMPETING COARSE REGISTRATION METHODS

Plots	Methods	Coarse registration errors			Success/Failure
		$E_R(rad)$	E_t(m)	E_p(m)	
1	TIN	0.040	0.524	0.695	✓
	2D-registration	0.085	0.849	1.184	✓
	SMST	0.021	0.230	0.258	✓
	GlobalMatch	0.020	0.211	0.247	✓
	MAC	0.038	0.579	0.691	✓
	PointNetLK	0.032	0.358	0.456	✓
2	TIN	0.042	0.632	0.725	✓
	2D-registration	0.061	0.226	0.780	✓
	SMST	0.032	0.365	0.475	✓
	GlobalMatch	0.033	0.320	0.431	✓
	MAC	0.045	0.532	0.693	✓
	PointNetLK	0.137	0.965	1.630	✗
3	TIN	0.061	0.505	0.946	✓
	2D-registration	0.051	0.567	0.675	✓
	SMST	0.042	0.632	0.725	✓
	GlobalMatch	0.047	0.553	0.691	✓
	MAC	1.016	42.882	8.255	✗
	PointNetLK	0.219	0.167	1.142	✗
4	TIN	0.133	12.594	7.059	✗
	2D-registration	0.690	44.096	50.219	✗
	SMST	0.474	60.701	16.643	✗
	GlobalMatch	1.571	277.179	58.247	✗
	MAC	0.694	65.758	38.258	✗
	PointNetLK	0.062	0.769	1.068	✓
5	TIN	2.154	85.098	29.385	✗
	2D-registration	0.890	86.779	20.387	✗
	SMST	2.036	93.425	22.176	✗
	GlobalMatch	0.047	0.874	0.787	✓
	MAC	0.046	0.794	0.835	✓
	PointNetLK	0.164	2.603	3.445	✗
6	TIN	1.340	10.445	25.681	✗
	2D-registration	0.200	3.123	4.199	✗
	SMST	1.571	26.634	36.030	✗
	GlobalMatch	3.098	15.741	35.641	✗
	MAC	0.039	0.865	0.700	✓
	PointNetLK	0.309	1.296	2.047	✗

two datasets and the higher accuracy of the collected data. Although the E_R value for the fine registration of Plot 2 is slightly larger than that of the coarse registration, the overall registration result after fine registration is much better when considering the other four metrics, which aligns with the visual effect shown in Fig. 7.

V. DISCUSSION

A. Comparison Experiments

To further evaluate the performance of our method, we conducted a comparative analysis with six existing registration methods, including TIN [31], 2-D-registration [32], stepwise minimum spanning tree (SMST) [34], GlobalMatch [49], maximal cliques (MAC) [69], as well as a deep learning-based method, PointNetLK [54]. The coarse registration accuracy of these methods is summarized in Table VII.

TIN is a method for fusing multiplatform LiDAR data based on the irregular triangular networks constructed from tree locations; 2-D-registration is a method for 2-D coarse registration of large-scale multisource forest point clouds by leveraging the distance relationship between neighboring trees within the specified search radius; SMST enables the registration of vehicle-borne and backpack LiDAR data by iteratively identifying common MST subgraphs of tree locations; GlobalMatch is a local-to-global registration method that iteratively refines initially paired local triangular facets to establish unique correspondences. For performance evaluation, the same tree locations were used as input for these methods. As shown in Table VII, four referenced methods (i.e., TIN, 2-D-registration, SMST, and GlobalMatch) successfully accomplished registration in Plots 1–3 (forests dominated by conifers) with average pointwise errors of 0.789, 0.880, 0.486, and 0.456 m, respectively. However, these methods faced challenges in registering sample plots dominated by broadleaf forests (Plots 4–6). Only the GlobalMatch method successfully achieved registration on Plot 5, which may be attributed to

the overall higher accuracy of individual tree detection on Plot 5 compared to Plots 4 and 6. The primary reason for the failure of these methods is rooted in the fact that the tree tops and trunks are not vertically aligned in broadleaf forests, coupled with the presence of heavy outliers in tree location data, thereby constraining the applicability of these methods within such environments.

MAC is a method for point cloud registration that leverages MAC. The key innovation of MAC is relaxing the previous maximum clique constraint to extract more local consensus information from the graph. We used the forest sample data from this article as input for the MAC method and evaluated the registration results. As shown in Table VII, MAC successfully achieved registration in Plots 1, 2, 5, and 6 but failed in Plots 3 and 4. Due to the strong dependence of the extracted geometric feature points on physical overlap, the MAC method cannot fully leverage its advantages in the low-overlap (less than 10%) forest scenes used in our study.

PointNetLK is a classical deep learning framework designed for point cloud registration, exhibiting reasonable generalization performance and still achieving good registration for untrained objects. However, previous studies reported that the PointNetLK algorithm only works for the transformations of small-scale point clouds [55] and necessitates central normalization of the point clouds when aligning large-scale outdoor scenes [34]. Our findings corroborate these constraints, as we observed that the PointNetLK algorithm yielded only acceptable results when the point densities of the two datasets were resampled to be more similar to each other. As indicated in Table VII, PointNetLK successfully achieved registration in Plots 1 and 4. In contrast, our algorithm effectively aligns large-scale outdoor point clouds without the need for central normalization or resampling.

Observations indicate that our method's coarse registration accuracy outperforms that of the six comparative methods across all six sample plots, demonstrating the effectiveness of the proposed method.

B. Sensitivity Analysis

Our method incorporates six parameters that require specific settings, as detailed in Table IV. These parameters can be harmonized under the general principle that smaller values are preferred for coniferous forests, while larger values are more suitable for broadleaf forests. For the parameters T_λ, T_μ, and T_ε, one can adopt parameter settings based on our previous work [34]. For new datasets, we recommend settings T_λ and T_μ to approximately 0.8 m and 8° for conifer-dominated forests, and 2 m and 12° for broadleaf-dominated forests, respectively. For parameter T_ε, a uniform setting of about 3 m is recommended. Since the sensitivity of these three parameters has been analyzed in our previous study, the current emphasis is on the remaining parameters.

The initial quadrant searching window size, T_g, exerts a significant influence on the registration result, and should not exceed the average crown diameter of the trees. We investigated the sensitivity of our method to variations in T_g under different forest environments, using Plot 1 (urban coniferous forest), Plot 4 (urban broadleaf forest), and Plot 6 (natural broadleaf forest) as case studies. Keeping all other parameters constant, we incrementally adjusted T_g and reran the algorithm. For Plot 1, T_g was initially set to 0.1 and increased from 0.25 to 1.75 with a step size of 0.25. From Fig. 8(a)–(c), it is evident that the registration accuracy stabilizes around 0.25, and the errors reach a local minimum of 1.25, with a trend of increasing errors beyond 1.5. This trend is consistent for E_R, E_t, and E_p. For Plot 4, T_g was increased from 0.5 to 4 in steps of 0.5. From Fig. 8(d)–(f), it is clear that the algorithm fails when T_g is small (0.5). As T_g increases, the registration accuracy begins to stabilize from 1, and the errors reach a local minimum at 2 and increase from 3. This pattern is also consistent across E_R, E_t, and E_p. For Plot 6, T_g was increased from 1 to 2.75 with a step size of 0.25. From Fig. 8(g)–(i), as T_g increases, the registration accuracy stabilizes from 1.25, and the errors reach a local minimum of 2 and depict an increasing trend from 2.5. This pattern is also consistent across E_R, E_t, and E_p. Overall, as the parameter T_g increases, the registration error exhibits a "U"-shaped distribution across all datasets. Therefore, we recommend setting T_g to approximately 1 m for new datasets dominated by coniferous forests and about 2 m for those dominated by broadleaf forests.

The initial average distance threshold T_d between matched node pairs is initially set to 1 and 1.5 for coniferous-dominated and broadleaf-dominated forests, respectively. This threshold is progressively decreased in subsequent iterations to refine the final transformation. Based on iterative trial-and-error experiments, we recommend setting T_d slightly smaller than T_g for new datasets.

The parameter T_N, which denotes the number of iterations in the quadrant searching process, was uniformly set to 3 in this study to avoid overly strict constraints that might impede convergence or lead to convergence to a local optimum. For new datasets, T_N can be adjusted based on the number of matched node pairs and the average distance between them in the output of each iteration, we recommend setting T_N to 3.

Individual tree detection is the prerequisite for the proposed method, and incorrect or missed detections might considerably influence the registration accuracy. To further evaluate the influence of the individual tree detection results on registration accuracy, we conducted a sensitivity analysis in a typical broadleaf forest (Plot 4). The F-scores of the individual tree detection results for both ULS and BLS were artificially manipulated by randomly removing or adding errors in this plot, decreasing from 1 to 0.3. As shown in Fig. 9, the number of successfully matched tree pairs gradually decreases as the F-scores decrease. The experimental results suggest that our registration algorithm is likely to achieve a high degree of success when the F-scores for both ULS and BLS datasets maintain a value of at least 0.4.

C. Computational Efficiency Analysis

Achieving the registration of airborne and ground point clouds in forest environments has always been challenging, especially in broadleaf forest scenarios. Therefore, we introduced a quadrant searching strategy driven by a heuristic algorithm to continuously optimize the registration

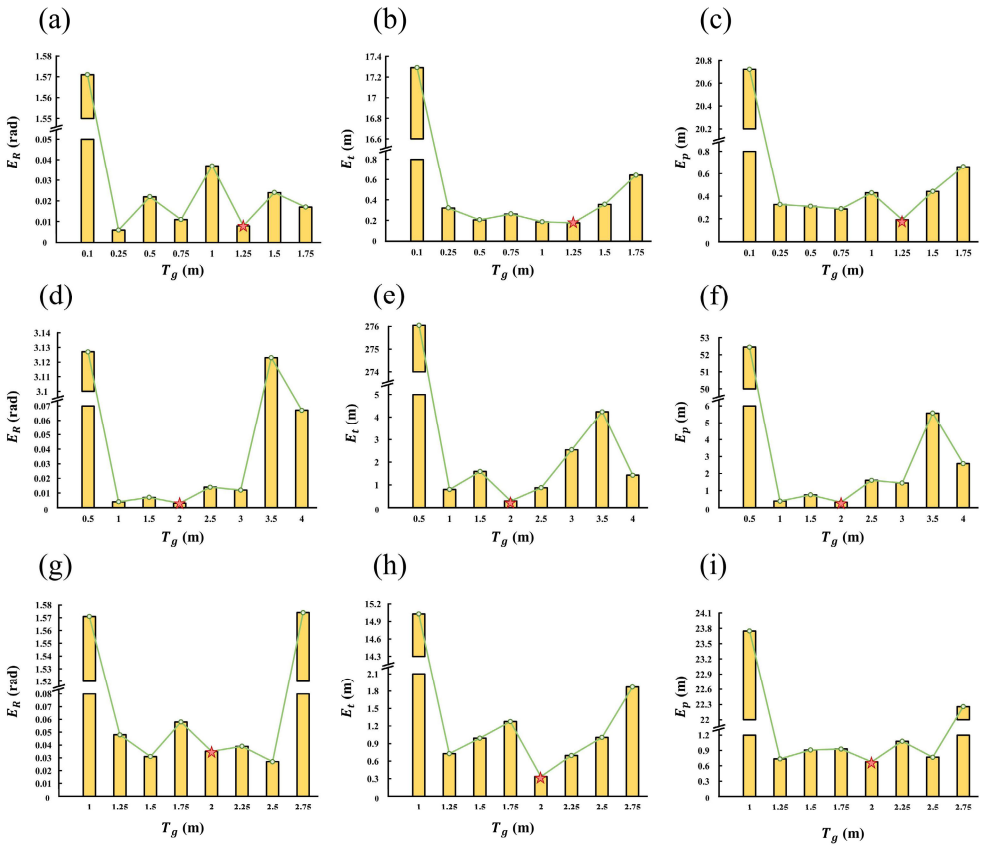

Fig. 8. Sensitivity analysis of the parameter T_g for (a)–(c) Plot 1, (d)–(f) Plot 4, and (g)–(i) Plot 6. The red pentagram represents the parameter values used in this study.

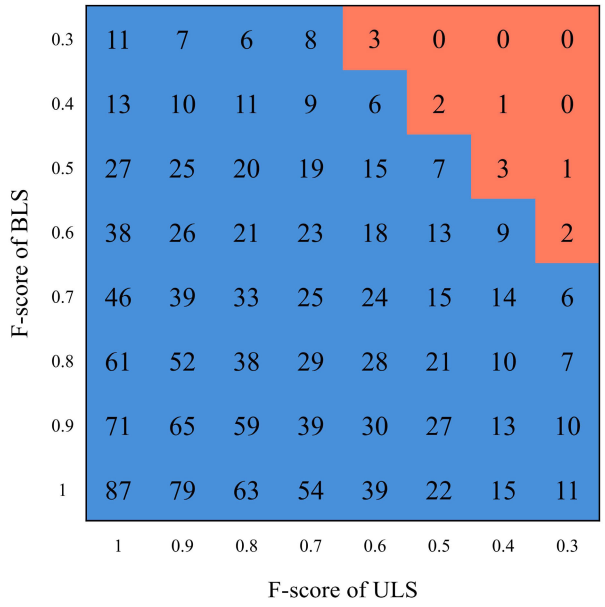

Fig. 9. Impacts of the individual tree detection accuracy on registration accuracy. The number in the box represents the number of matched tree pairs, with a blue background representing successful registration, whereas a red background denotes registration failures.

results, which can effectively retain more potential matching correspondences and significantly improve the success rate of registration. In our study, the computational time for the execution of the quadrant search-based MST matching algorithm on a 12-core CPU using parallel computing ranges from 1.4 to 17.5 min for six sample plots. The execution time of the MST matching process, including MST construction, node similarity matching, correspondence pruning, and correspondence expansion, is notably rapid. The measured times for these steps were 1.365, 1.231, 2.965, 2.836, 4.179, and 0.625 s, respectively. Although the quadrant search process somewhat diminishes the computational efficiency of our method, the time consumed by our method is still acceptable.

D. Limitations and Outlooks

The proposed method achieved satisfactory registration results in forested areas, but two limitations require consideration in future studies. First, as shown in Fig. 10, the MST [Fig. 10(a)] marked in blue is constructed using the ULS tree locations obtained through quadrant searching, while the MST [Fig. 10(b)] marked in red is constructed using the BLS tree locations. The figure illustrates a scenario where there are fewer than four topologically similar tree locations (indicated by black-bordered points) between the two MSTs. In such a case, neither a robust triangle nor common subgraphs can be constructed, leading to an increased rate of registration failure. Future studies can explore the possibility of matching approaches that allow the coexistence of multiple graph

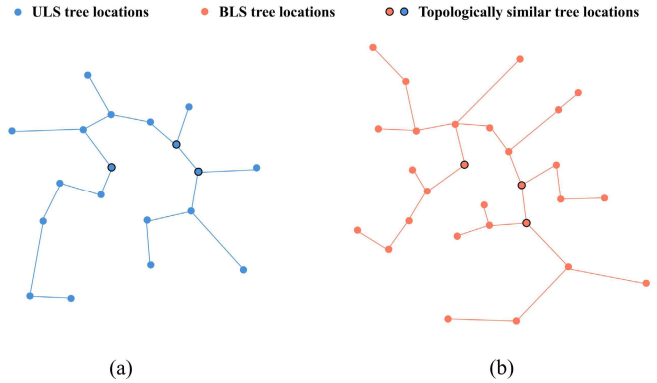

Fig. 10. Illustration of registration failure with fewer than four topologically similar trees. (a) and (b) Tree location maps constructed from ULS and BLS, respectively.

structures. Second, the proposed method shares a common limitation with other tree location-based methods, where incorrect matching may occur for trees arranged in a regular pattern. To address this, it is recommended to chunk the two sets of tree location maps before matching and crop out the irregularly arranged sections for registration. The resulting transformation matrix can then be applied to the entire point cloud. Besides, we found the MAC method [69] offers valuable inspiration for further accelerating the correspondence pruning process. In future work, we propose randomly generating triangle constraint feature descriptors for the initial correspondences, followed by selecting the best match as the output based on scoring and ranking each match. This approach maximizes the retention of the best matches and would further improve the algorithm's robustness compared to the previous method, which performed descriptor matching sequentially and outputted the first match that satisfied the threshold.

VI. Conclusion

In this study, we have proposed *QuadrantSearch*, a novel registration method for UAV and backpack LiDAR data in both urban and natural forests. *QuadrantSearch* requires only the tree locations detected from the point clouds as input, without necessitating other tree attribute information. The quadrant searching strategy takes into account the inherent differences between tree tops and trunks and effectively aligns both coniferous and broadleaf forest point clouds. Additionally, we have introduced a robust triangle constraint algorithm to enhance applicability in cases where the individual tree detection algorithm may be less effective. Registration is achieved by identifying only four discrete, topologically similar trees in two tree location maps. Moreover, the optimal transformation search step, which employs a heuristic genetic algorithm, reduces the solution space and yields better results than the exhaustive-search style approach. Our method demonstrates superior accuracy in comparison to six other competing techniques across all six sample plots. Importantly, our proposed method exhibits robustness to user-defined parameter settings, with the window size of the quadrant searching being the sole parameter requiring iterative adjustment.

Looking forward, we are confident that our method can be applied to register point clouds from various ground-based LiDAR platforms (e.g., terrestrial, backpack, and handheld platforms) in both urban and natural forests with high accuracy. Furthermore, our method shows potential for extension to other application scenarios, where the tree locations can be replaced by other tie points without necessitating high accuracy.

References

[1] B. Wu et al., "A voxel-based method for automated identification and morphological parameters estimation of individual street trees from mobile laser scanning data," *Remote Sens.*, vol. 5, no. 2, pp. 584–611, Jan. 2013, doi: 10.3390/rs5020584.

[2] S. Gao, Z. Zhang, and L. Cao, "Individual tree structural parameter extraction and volume table creation based on near-field LiDAR data: A case study in a subtropical planted forest," *Sensors*, vol. 21, no. 23, p. 8162, Dec. 2021, doi: 10.3390/s21238162.

[3] D. Panagiotidis, A. Abdollahnejad, and M. Slavík, "3D point cloud fusion from UAV and TLS to assess temperate managed forest structures," *Int. J. Appl. Earth Observ. Geoinf.*, vol. 112, Aug. 2022, Art. no. 102917, doi: 10.1016/j.jag.2022.102917.

[4] C. Li, Z. Chen, X. Zhou, M. Zhou, and Z. Li, "Generalized models for subtropical forest inventory attribute estimations using a rule-based exhaustive combination approach with airborne LiDAR-derived metrics," *GIScience Remote Sens.*, vol. 60, no. 1, Apr. 2023, Art. no. 2194601, doi: 10.1080/15481603.2023.2194601.

[5] R. Fekry, W. Yao, L. Cao, and X. Shen, "Ground-based/UAV-LiDAR data fusion for quantitative structure modeling and tree parameter retrieval in subtropical planted forest," *Forest Ecosyst.*, vol. 9, Sep. 2022, Art. no. 100065, doi: 10.1016/j.fecs.2022.100065.

[6] S. Hu, Z. Li, Z. Zhang, D. He, and M. Wimmer, "Efficient tree modeling from airborne LiDAR point clouds," *Comput. Graph.*, vol. 67, pp. 1–13, Oct. 2017, doi: 10.1016/j.cag.2017.04.004.

[7] D. Kelbe, J. van Aardt, P. Romanczyk, M. van Leeuwen, and K. Cawse-Nicholson, "Single-scan stem reconstruction using low-resolution terrestrial laser scanner data," *IEEE J. Sel. Topics Appl. Earth Observ. Remote Sens.*, vol. 8, no. 7, pp. 3414–3427, Jul. 2015, doi: 10.1109/JSTARS.2015.2416001.

[8] S. Yu et al., "View-based greenery: A three-dimensional assessment of city buildings' green visibility using floor green view index," *Landscape Urban Planning*, vol. 152, pp. 13–26, Aug. 2016, doi: 10.1016/j.landurbplan.2016.04.004.

[9] Y. Huang et al., "Toward automatic estimation of urban green volume using airborne LiDAR data and high resolution remote sensing images," *Frontiers Earth Sci.*, vol. 7, no. 1, pp. 43–54, Mar. 2013, doi: 10.1007/s11707-012-0339-6.

[10] X. Liang et al., "Terrestrial laser scanning in forest inventories," *ISPRS J. Photogramm. Remote Sens.*, vol. 115, pp. 63–77, May 2016, doi: 10.1016/j.isprsjprs.2016.01.006.

[11] P. R. Stephens et al., "Airborne scanning LiDAR in a double sampling forest carbon inventory," *Remote Sens. Environ.*, vol. 117, pp. 348–357, Feb. 2012, doi: 10.1016/j.rse.2011.10.009.

[12] B. Brede et al., "Non-destructive estimation of individual tree biomass: Allometric models, terrestrial and UAV laser scanning," *Remote Sens. Environ.*, vol. 280, Oct. 2022, Art. no. 113180, doi: 10.1016/j.rse.2022.113180.

[13] M. A. Wulder, C. W. Bater, N. C. Coops, T. Hilker, and J. C. White, "The role of LiDAR in sustainable forest management," *Forestry Chronicle*, vol. 84, no. 6, pp. 807–826, Dec. 2008, doi: 10.5558/tfc84807-6.

[14] S. Dakin Kuiper, N. C. Coops, L. R. Jarron, P. Tompalski, and J. C. White, "An automated approach to detecting instream wood using airborne laser scanning in small coastal streams," *Int. J. Appl. Earth Observ. Geoinformation*, vol. 118, Apr. 2023, Art. no. 103272, doi: 10.1016/j.jag.2023.103272.

[15] B. Wu, B. Yu, Q. Wu, Y. Huang, Z. Chen, and J. Wu, "Individual tree crown delineation using localized contour tree method and airborne LiDAR data in coniferous forests," *Int. J. Appl. Earth Observ. Geoinf.*, vol. 52, pp. 82–94, Oct. 2016, doi: 10.1016/j.jag.2016.06.003.

[16] I. Korpela, A. Hovi, and F. Morsdorf, "Understory trees in airborne LiDAR data—Selective mapping due to transmission losses and echo-triggering mechanisms," *Remote Sens. Environ.*, vol. 119, pp. 92–104, Apr. 2012, doi: 10.1016/j.rse.2011.12.011.

[17] J. Shao et al., "Single scanner BLS system for forest plot mapping," *IEEE Trans. Geosci. Remote Sens.*, vol. 59, no. 2, pp. 1675–1685, Feb. 2021, doi: 10.1109/TGRS.2020.2999413.

[18] F. Tupinambá-Simões, A. Pascual, J. Guerra-Hernández, C. Ordóñez, T. de Conto, and F. Bravo, "Assessing the performance of a handheld laser scanning system for individual tree mapping—A mixed forests showcase in Spain," *Remote Sens.*, vol. 15, no. 5, p. 1169, Feb. 2023, doi: 10.3390/rs15051169.

[19] H. Kaartinen et al., "Accuracy of kinematic positioning using global satellite navigation systems under forest canopies," *Forests*, vol. 6, no. 12, pp. 3218–3236, Sep. 2015, doi: 10.3390/f6093218.

[20] T. Zhou, R. Ravi, Y.-C. Lin, R. Manish, S. Fei, and A. Habib, "In situ calibration and trajectory enhancement of UAV and backpack LiDAR systems for fine-resolution forest inventory," *Remote Sens.*, vol. 15, no. 11, p. 2799, May 2023, doi: 10.3390/rs15112799.

[21] C. Paris, D. Kelbe, J. van Aardt, and L. Bruzzone, "A novel automatic method for the fusion of ALS and TLS LiDAR data for robust assessment of tree crown structure," *IEEE Trans. Geosci. Remote Sens.*, vol. 55, no. 7, pp. 3679–3693, Jul. 2017, doi: 10.1109/TGRS.2017.2675963.

[22] Y. Zhao, J. Im, Z. Zhen, and Y. Zhao, "Towards accurate individual tree parameters estimation in dense forest: Optimized coarse-to-fine algorithms for registering UAV and terrestrial LiDAR data," *GISci. Remote Sens.*, vol. 60, no. 1, Apr. 2023, Art. no. 2197281, doi: 10.1080/15481603.2023.2197281.

[23] L. Cheng, Y. Wu, L. Tong, Y. Chen, and M. Li, "Hierarchical registration method for airborne and vehicle LiDAR point cloud," *Remote Sens.*, vol. 7, no. 10, pp. 13921–13944, Oct. 2015, doi: 10.3390/rs71013921.

[24] L. Cheng, L. Tong, Y. Wu, Y. Chen, and M. Li, "Shiftable leading point method for high accuracy registration of airborne and terrestrial LiDAR data," *Remote Sens.*, vol. 7, no. 2, pp. 1915–1936, Feb. 2015, doi: 10.3390/rs70201915.

[25] B. Yang, Y. Zang, Z. Dong, and R. Huang, "An automated method to register airborne and terrestrial laser scanning point clouds," *ISPRS J. Photogramm. Remote Sens.*, vol. 109, pp. 62–76, Nov. 2015, doi: 10.1016/j.isprsjprs.2015.08.006.

[26] F. Liang, B. Yang, Z. Dong, R. Huang, Y. Zang, and Y. Pan, "A novel skyline context descriptor for rapid localization of terrestrial laser scans to airborne laser scanning point clouds," *ISPRS J. Photogramm. Remote Sens.*, vol. 165, pp. 120–132, Jul. 2020, doi: 10.1016/j.isprsjprs.2020.04.018.

[27] B. Yang, Z. Dong, F. Liang, and Y. Liu, "Automatic registration of large-scale urban scene point clouds based on semantic feature points," *ISPRS J. Photogramm. Remote Sens.*, vol. 113, pp. 43–58, Mar. 2016, doi: 10.1016/j.isprsjprs.2015.12.005.

[28] P. Wei, L. Yan, H. Xie, and M. Huang, "Automatic coarse registration of point clouds using plane contour shape descriptor and topological graph voting," *Autom. Construct.*, vol. 134, Feb. 2022, Art. no. 104055, doi: 10.1016/j.autcon.2021.104055.

[29] O. Pohjavirta et al., "Automated registration of wide-baseline point clouds in forests using discrete overlap search," *Forest Ecosyst.*, vol. 9, May 2022, Art. no. 100080, doi: 10.1016/j.fecs.2022.100080.

[30] P. Polewski, W. Yao, L. Cao, and S. Gao, "Marker-free coregistration of UAV and backpack LiDAR point clouds in forested areas," *ISPRS J. Photogramm. Remote Sens.*, vol. 147, pp. 307–318, Jan. 2019, doi: 10.1016/j.isprsjprs.2018.11.020.

[31] H. Guan et al., "A novel framework to automatically fuse multiplatform LiDAR data in forest environments based on tree locations," *IEEE Trans. Geosci. Remote Sens.*, vol. 58, no. 3, pp. 2165–2177, Mar. 2020, doi: 10.1109/TGRS.2019.2953654.

[32] E. Hyyppä, J. Muhojoki, X. Yu, A. Kukko, H. Kaartinen, and J. Hyyppä, "Efficient coarse registration method using translation- and rotation-invariant local descriptors towards fully automated forest inventory," *ISPRS Open J. Photogramm. Remote Sens.*, vol. 2, Dec. 2021, Art. no. 100007, doi: 10.1016/j.ophoto.2021.100007.

[33] W. Dai et al., "Multisource forest point cloud registration with semantic-guided keypoints and robust RANSAC mechanisms," *Int. J. Appl. Earth Observ. Geoinf.*, vol. 115, Dec. 2022, Art. no. 103105, doi: 10.1016/j.jag.2022.103105.

[34] B. Wu et al., "A stepwise minimum spanning tree matching method for registering vehicle-borne and backpack LiDAR point clouds," *IEEE Trans. Geosci. Remote Sens.*, vol. 60, 2022, Art. no. 5705713, doi: 10.1109/TGRS.2022.3226956.

[35] H. Chen and B. Bhanu, "3D free-form object recognition in range images using local surface patches," *Pattern Recognit. Lett.*, vol. 28, no. 10, pp. 1252–1262, Jul. 2007, doi: 10.1016/j.patrec.2007.02.009.

[36] Y. Zhong, "Intrinsic shape signatures: A shape descriptor for 3D object recognition," in *Proc. IEEE 12th Int. Conf. Comput. Vis. Workshops, ICCV Workshops*, Kyoto, Japan, Sep. 2009, pp. 689–696.

[37] A. Zaharescu, E. Boyer, K. Varanasi, and R. Horaud, "Surface feature detection and description with applications to mesh matching," in *Proc. IEEE Conf. Comput. Vis. Pattern Recognit.*, Miami, FL, USA, Jun. 2009, pp. 373–380.

[38] T.-W.-R. Lo and J. P. Siebert, "Local feature extraction and matching on range images: 2.5D SIFT," *Comput. Vis. Image Understand.*, vol. 113, no. 12, pp. 1235–1250, Dec. 2009, doi: 10.1016/j.cviu.2009.06.005.

[39] J. Knopp, M. Prasad, G. Willems, R. Timofte, and L. Van Gool, "Hough transform and 3D SURF for robust three dimensional classification," in *Proc. 11th Eur. Conf. Comput. Vis. (ECCV)*, Heraklion, Greece, Sep. 2010, pp. 589–602.

[40] I. Sipiran and B. Bustos, "Harris 3D: A robust extension of the Harris operator for interest point detection on 3D meshes," *Vis. Comput.*, vol. 27, no. 11, pp. 963–976, Jul. 2011, doi: 10.1007/s00371-011-0610-y.

[41] J. Shao et al., "Efficient co-registration of UAV and ground LiDAR forest point clouds based on canopy shapes," *Int. J. Appl. Earth Observ. Geoinf.*, vol. 114, Nov. 2022, Art. no. 103067, doi: 10.1016/j.jag.2022.103067.

[42] X. Ge, Z. Han, Q. Zhu, H. Hu, B. Xu, and M. Chen, "CPS: A novel canopy profile skyline descriptor for UAV and terrestrial-based forest point cloud registration," *Int. J. Appl. Earth Observ. Geoinf.*, vol. 130, Jun. 2024, Art. no. 103928, doi: 10.1016/j.jag.2024.103928.

[43] W. Dai et al., "Automated fusion of forest airborne and terrestrial point clouds through canopy density analysis," *ISPRS J. Photogramm. Remote Sens.*, vol. 156, pp. 94–107, Oct. 2019, doi: 10.1016/j.isprsjprs.2019.08.008.

[44] H. Guan et al., "A marker-free method for registering multi-scan terrestrial laser scanning data in forest environments," *ISPRS J. Photogramm. Remote Sens.*, vol. 166, pp. 82–94, Aug. 2020, doi: 10.1016/j.isprsjprs.2020.06.002.

[45] D. Kelbe, J. van Aardt, P. Romanczyk, M. van Leeuwen, and K. Cawse-Nicholson, "Marker-free registration of forest terrestrial laser scanner data pairs with embedded confidence metrics," *IEEE Trans. Geosci. Remote Sens.*, vol. 54, no. 7, pp. 4314–4330, Jul. 2016, doi: 10.1109/TGRS.2016.2539219.

[46] J.-F. Tremblay and M. Béland, "Towards operational marker-free registration of terrestrial lidar data in forests," *ISPRS J. Photogramm. Remote Sens.*, vol. 146, pp. 430–435, Dec. 2018, doi: 10.1016/j.isprsjprs.2018.10.011.

[47] Q. Liu et al., "Target-free ULS-TLS point-cloud registration for Alpine forest lands," *Comput. Electron. Agricult.*, vol. 190, Nov. 2021, Art. no. 106460, doi: 10.1016/j.compag.2021.106460.

[48] X. Ge, Q. Zhu, L. Huang, S. Li, and S. Li, "Global registration of multiview unordered forest point clouds guided by common subgraphs," *IEEE Trans. Geosci. Remote Sens.*, vol. 60, 2022, Art. no. 5700214, doi: 10.1109/TGRS.2021.3057643.

[49] X. Wang et al., "GlobalMatch: Registration of forest terrestrial point clouds by global matching of relative stem positions," *ISPRS J. Photogramm. Remote Sens.*, vol. 197, pp. 71–86, Mar. 2023, doi: 10.1016/j.isprsjprs.2023.01.013.

[50] Z. Dong et al., "Registration of large-scale terrestrial laser scanner point clouds: A review and benchmark," *ISPRS J. Photogramm. Remote Sens.*, vol. 163, pp. 327–342, May 2020, doi: 10.1016/j.isprsjprs.2020.03.013.

[51] B. Yang, X. Han, and Z. Dong, "Point cloud benchmark dataset WHU-TLS and WHU-MLS for deep learning," *J. Remote Sens.*, vol. 25, no. 1, pp. 231–240, Jan. 2021, doi: 10.11834/jrs.20210542.

[52] R. Q. Charles, H. Su, M. Kaichun, and L. J. Guibas, "PointNet: Deep learning on point sets for 3D classification and segmentation," in *Proc. IEEE Conf. Comput. Vis. Pattern Recognit. (CVPR)*, Honolulu, HI, USA, Jul. 2017, pp. 652–660.

[53] C. R. Qi, L. Yi, H. Su, and L. J. Guibas, "PointNet++: Deep hierarchical feature learning on point sets in a metric space," in *Proc. 31st Int. Adv. Neural Inf. Process. Syst.*, Long Beach, CA, USA, Dec. 2017, pp. 5099–5108.

[54] Y. Aoki, H. Goforth, R. A. Srivatsan, and S. Lucey, "PointNetLK: Robust & efficient point cloud registration using PointNet," in *Proc. IEEE/CVF Conf. Comput. Vis. Pattern Recognit. (CVPR)*, Long Beach, CA, USA, Jun. 2019, pp. 7156–7165.

[55] Y. Wang and J. Solomon, "Deep closest point: Learning representations for point cloud registration," in *Proc. IEEE/CVF Int. Conf. Comput. Vis. (ICCV)*, Seoul, South Korea, Oct. 2019, pp. 3522–3531.

[56] Y. Wang, B. Yang, Y. Chen, F. Liang, and Z. Dong, "JoKDNet: A joint keypoint detection and description network for large-scale outdoor TLS point clouds registration," *Int. J. Appl. Earth Observ. Geoinf.*, vol. 104, Dec. 2021, Art. no. 102534, doi: 10.1016/j.jag.2021.102534.

[57] H. Wang et al., "RoReg: Pairwise point cloud registration with oriented descriptors and local rotations," *IEEE Trans. Pattern Anal. Mach. Intell.*, vol. 45, no. 8, pp. 10376–10393, Aug. 2023, doi: 10.1109/TPAMI.2023.3244951.

[58] Z. Deng, Y. Yao, B. Deng, and J. Zhang, "A robust loss for point cloud registration," in *Proc. IEEE/CVF Int. Conf. Comput. Vis. (ICCV)*, Montreal, QC, Canada, Oct. 2021, pp. 6118–6127.

[59] H. Yang, J. Shi, and L. Carlone, "TEASER: Fast and certifiable point cloud registration," *IEEE Trans. Robot.*, vol. 37, no. 2, pp. 314–333, Apr. 2021, doi: 10.1109/TRO.2020.3033695.

[60] S. Tao et al., "Segmenting tree crowns from terrestrial and mobile LiDAR data by exploring ecological theories," *ISPRS J. Photogramm. Remote Sens.*, vol. 110, pp. 66–76, Dec. 2015, doi: 10.1016/j.isprsjprs.2015.10.007.

[61] E. Ayrey et al., "Layer stacking: A novel algorithm for individual forest tree segmentation from LiDAR point clouds," *Can. J. Remote Sens.*, vol. 43, no. 1, pp. 16–27, Jan. 2017, doi: 10.1080/07038992.2017.1252907.

[62] R. C. Prim, "Shortest connection networks and some generalizations," *Bell Syst. Tech. J.*, vol. 36, no. 6, pp. 1389–1401, Nov. 1957, doi: 10.1002/j.1538-7305.1957.tb01515.x.

[63] B. Wu et al., "An extended minimum spanning tree method for characterizing local urban patterns," *Int. J. Geograph. Inf. Sci.*, vol. 32, no. 3, pp. 450–475, Mar. 2018, doi: 10.1080/13658816.2017.1384830.

[64] B. Wu et al., "A graph-based approach for 3D building model reconstruction from airborne LiDAR point clouds," *Remote Sens.*, vol. 9, no. 1, p. 92, Jan. 2017, doi: 10.3390/rs9010092.

[65] J. Kostensalo, L. Mehtätalo, S. Tuominen, P. Packalen, and M. Myllymäki, "Recreating structurally realistic tree maps with airborne laser scanning and ground measurements," *Remote Sens. Environ.*, vol. 298, Dec. 2023, Art. no. 113782, doi: 10.1016/j.rse.2023.113782.

[66] W. Zhang et al., "An easy-to-use airborne LiDAR data filtering method based on cloth simulation," *Remote Sens.*, vol. 8, no. 6, p. 501, Jun. 2016, doi: 10.3390/rs8060501.

[67] T. Papadopoulo and M. I. A. Lourakis, "Estimating the Jacobian of the singular value decomposition: Theory and applications," in *Proc. 6th Eur. Conf. Comput. Vis. (ECCV)*, Jun. 2000, pp. 554–570.

[68] P. J. Besl and N. D. McKay, "A method for registration of 3-D shapes," *IEEE Trans. Pattern Anal. Mach. Intell.*, vol. 14, no. 2, pp. 239–256, Feb. 1992, doi: 10.1109/34.121791.

[69] X. Zhang, J. Yang, S. Zhang, and Y. Zhang, "3D registration with maximal cliques," in *Proc. IEEE/CVF Conf. Comput. Vis. Pattern Recognit. (CVPR)*, Vancouver, BC, Canada, Jun. 2023, pp. 17745–17754.

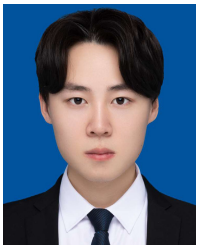

Guorong Li received the B.S. degree in geographic information science (GIS) from Shandong University of Science and Technology, Qingdao, China, in 2022. He is currently pursuing the M.S. degree in geomatics engineering with the Key Laboratory of Geographic Information Science (Ministry of Education), School of Geographic Sciences, East China Normal University, Shanghai, China.

His research interests include urban remote sensing and light detection and ranging (LiDAR).

Bin Wu (Member, IEEE) received the Ph.D. degree in cartography and geographic information systems (GIS) from East China Normal University, Shanghai, China, in 2018.

He is currently an Associate Professor with the School of Geospatial Engineering and Science, Sun Yat-sen University, Zhuhai, China. His research interests include light detection and ranging (LiDAR), urban remote sensing, 3-D urban morphology, and spatiotemporal analysis.

Lei Yang received the B.S. degree in geographic information science (GIS) from Huazhong Agricultural University, Wuhan, China, in 2020, and the M.S. degree in geomatics engineering from the Key Laboratory of Geographic Information Science (Ministry of Education), School of Geographic Sciences, East China Normal University, Shanghai, China, in 2023.

His research interests include urban remote sensing and light detection and ranging (LiDAR).

Zhan Pan received the B.S. degree in geographic information science (GIS) from Dalian Maritime University, Dalian, China, in 2021. He is currently pursuing the Ph.D. degree in cartography and geographic information systems with the Key Laboratory of Geographic Information Science (Ministry of Education), School of Geographic Sciences, East China Normal University, Shanghai, China.

His research interests include urban remote sensing and light detection and ranging (LiDAR).

Linxin Dong received the B.S. degree in remote sensing science and technology from Chengdu University of Technology, Chengdu, China, in 2022. She is currently pursuing the Ph.D. degree in cartography and geographic information systems with the Key Laboratory of Geographic Information Science (Ministry of Education), School of Geographic Sciences, East China Normal University, Shanghai, China.

Her research interests include spatiotemporal fusion and cryosphere remote sensing.

Siyu Wu received the B.S. degree in bioscience from Shanghai Normal University, Shanghai, China, in 2019. He is currently pursuing the Ph.D. degree in ecology with the School of Ecological and Environmental Sciences, East China Normal University, Shanghai.

His research focuses on forest diversity patterns and processes and 3-D reconstruction of forest scenes by near-ground unmanned aerial vehicle (UAV) remote sensing.

Guochun Shen received the Ph.D. degree from Zhejiang University, Zhejiang, China, in 2010.

He is currently a Professor with the School of Ecological and Environmental Sciences, East China Normal University, Shanghai, China. His research focuses on how and why species, especially subtropical forest trees, coexist in heterogeneous environments, and how can we accurately and robustly detect and estimate the effects of abiotic habitat, dispersal, and individual interaction on community structures from a spatially explicit perspective.

Jiarui Zhang received the B.S. degree in remote sensing science and technology from Shandong University of Science and Technology, Qingdao, China, in 2022. He is currently pursuing the M.S. degree in geomatics engineering with the Key Laboratory of Geographic Information Science (Ministry of Education), School of Geographic Sciences, East China Normal University, Shanghai, China.

His research interests include urban remote sensing, nighttime light remote sensing, and light detection and ranging (LiDAR).

Tian Xiao received the B.S. degree in geographic information science (GIS) from East China Normal University, Shanghai, China, in 2021, where he is currently pursuing the M.S. degree in cartography and geographic information systems with the Key Laboratory of Geographic Information Science (Ministry of Education), School of Geographic Sciences.

His research interests include urban remote sensing and light detection and ranging (LiDAR).

Lefeng Zhang received the B.S. degree in earth information science and technology from China University of Geosciences, Wuhan, China, in 2023. He is currently pursuing the M.S. degree in geomatics engineering with the Key Laboratory of Geographic Information Science (Ministry of Education), School of Geographic Sciences, East China Normal University, Shanghai, China.

His research interests include urban remote sensing and light detection and ranging (LiDAR).

Jianping Wu received the M.S. degree in cartography and remote sensing from Peking University, Beijing, China, in 1986, and the Ph.D. degree in regional geography from East China Normal University, Shanghai, China, in 1996.

He is currently a Professor with the Key Laboratory of Geographic Information Science (Ministry of Education), School of Geographic Sciences, East China Normal University. His research interests include remote sensing and geographic information systems.

Bailang Yu (Senior Member, IEEE) received the B.S. and Ph.D. degrees in cartography and geographic information systems from East China Normal University, Shanghai, China, in 2002 and 2009, respectively.

He is currently a Professor with the Key Laboratory of Geographic Information Science (Ministry of Education), East China Normal University, where he is also with the School of Geographic Sciences. His research interests include urban remote sensing, nighttime light remote sensing, light detection and ranging (LiDAR), and object-based methods.